Journal of Zhejiang University-SCIENCE A

Piezoelectric ultrasonic coupling-based polishing of micro-tapered holes with abrasive flow

Gaoan ZHENG, Xiaoxing WENG, Tong WANG, Pu XU, Weixin XU, Lin LI, Xuefeng XU, Dapeng TAN

Cite this as: Gaoan ZHENG, Xiaoxing WENG, Tong WANG, Pu XU, Weixin XU, Lin LI, Xuefeng XU, Dapeng TAN, 2025. Piezoelectric ultrasonic coupling-based polishing of micro-tapered holes with abrasive flow. *Journal of Zhejiang University-SCIENCE A*, 26(12):1141-1162.
https://doi.org/10.1631/jzus.A2400343

1 Introduction

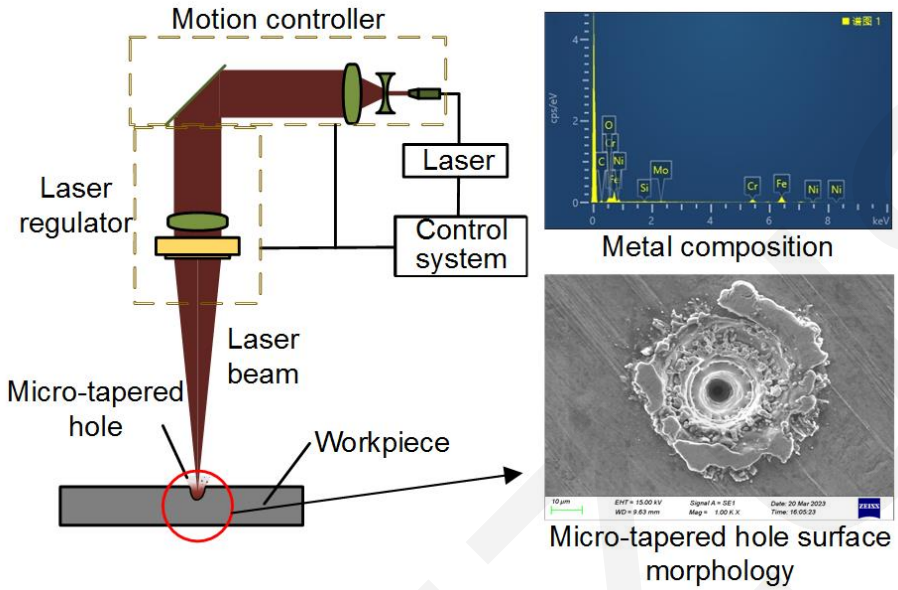

Fig.1 Principle of laser processing of micro-tapered holes and their surface morphology

Micro-tapered holes are the main sites for the mixing, reaction and separation of mesoscopic fluids, and also constitute the main structure of microfluidic chips. The surface quality of micro-conical holes directly affects the flow characteristics, mixing effect and analytical sensitivity of mesoscopic fluids. Micro-conical holes are mainly formed by laser processing, and the quality of their hole walls is often poor, as depicted in Fig. 1.

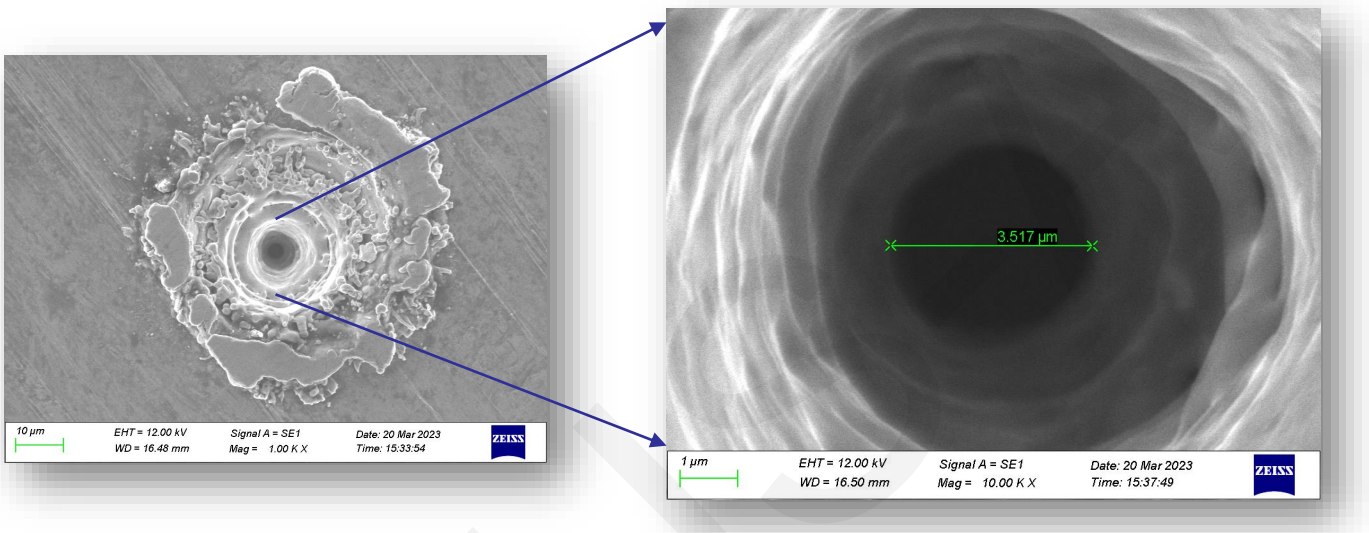

Fig.2 Internal morphology of the micro-tapered holes

The minimum diameter of the micro-tapered holes is only 3 µm (as depicted in Fig. 2), and the existing methods are difficult to effectively polish its inner wall. Therefore, this paper proposes an active multiphase field material removal method of piezoelectric ultrasonic coupled abrasive flow polishing (PU-AP). This method significantly enhances the kinetic energy of the fluid within the microstructure through the assistance of ultrasonic waves, thereby improving the polishing effect.

2 PU-AP theoretical model

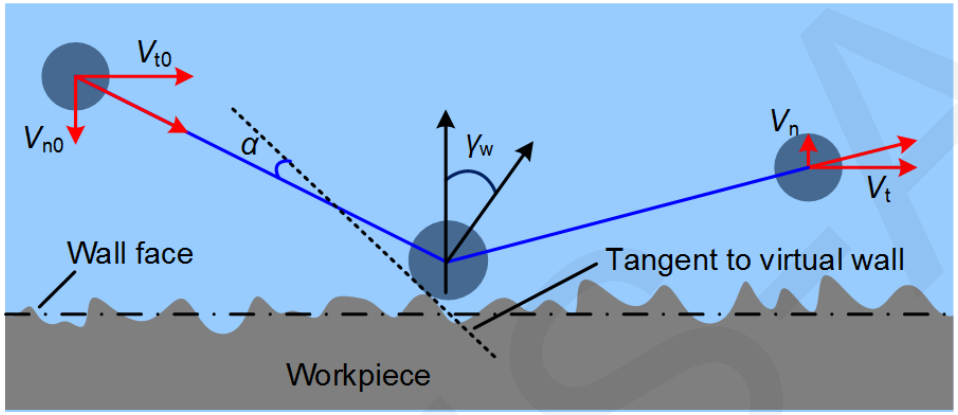

Fig. 3 Abrasive grain–wall impact erosion process.

k-ε Model

$$\frac{\partial(\rho k)}{\partial t}+\frac{\partial(\rho k\boldsymbol{v})}{\partial x_i}=\frac{\partial}{\partial x_j}\left[(\mu+\frac{\mu_t}{\sigma_k})\frac{\partial k}{\partial x_j}\right]+G_b+G_k-\rho\varepsilon+Y_M$$

$$\frac{\partial(\rho\varepsilon)}{\partial t}+\frac{\partial(\rho\varepsilon\boldsymbol{v})}{\partial x_i}=\frac{\partial}{\partial x_i}\left[\left(\mu+\frac{\mu_t}{\sigma_\varepsilon}\right)\frac{\partial\varepsilon}{\partial x_j}\right]+\rho C_1E\varepsilon-\rho C_2\frac{\varepsilon^2}{k+\sqrt{\nu\varepsilon}}$$

Continuity equation and momentum of each mesh

$$\nabla\cdot\boldsymbol{v}=0$$

$$\rho\frac{\partial\boldsymbol{v}}{\partial t}+\rho(\boldsymbol{v}\cdot\nabla)\boldsymbol{v}=-\nabla P+\nabla\cdot\left[\mu(\nabla\boldsymbol{v}+\nabla\boldsymbol{v}^{\mathrm{T}})\right]+\rho\boldsymbol{g}+\boldsymbol{F}$$

The path of abrasive particles

$$m_a\frac{\mathrm{d}\boldsymbol{v}_a}{\mathrm{d}t}=m_a\frac{18\mu}{\rho_a d_p^2}\frac{C_D Re_p(\boldsymbol{v}-\boldsymbol{v}_a)}{24}+m_a\frac{\boldsymbol{g}(\rho_a-\rho)}{\rho_a}+\frac{m_a\rho}{2\rho_a}\frac{d(\boldsymbol{v}-\boldsymbol{v}_a)}{dt}+\frac{5.188m_a\rho\sqrt{\nu}d_{ij}(\boldsymbol{v}-\boldsymbol{v}_a)}{\rho_a d_p\left(d_{lk}d_{kl}\right)^{1/4}}$$

$$m_e=E_r N_p m_p.$$

The amount of surface wear

$$E_r=k_r V_p^2 f(\gamma),$$

The Finnie model

$$e_n=\frac{V_n}{V_{n0}}=0.998-0.78\alpha+0.19\alpha^2-0.024\alpha^3+0.027\alpha^4,$$

$$e_t=\frac{V_t}{V_{t0}}=1-0.78\alpha+0.84\alpha^2-0.21\alpha^3+0.028\alpha^4-0.022\alpha^5,$$

The coefficient of recovery model

3 PU-AP modeling methodology

3.1 Principle of PU-AP processing

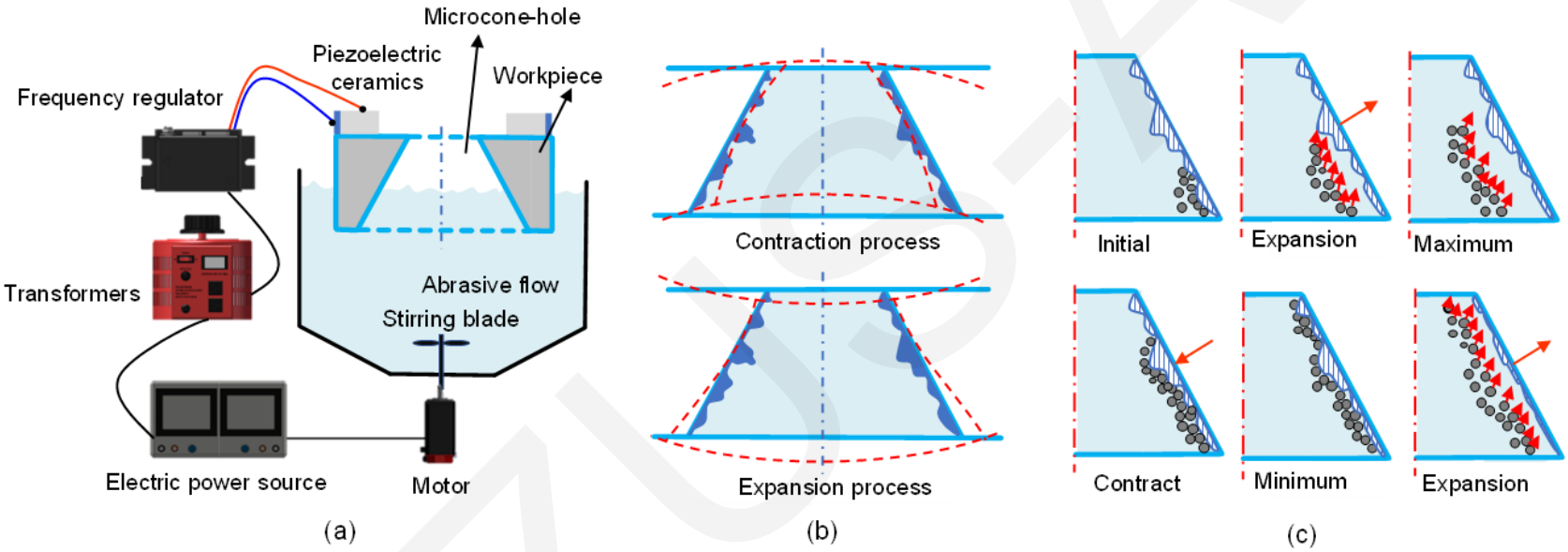

Fig. 4 PU-AP polishing principle: (a) schematic diagram; (b) asymptotic expansion–contraction process; (c) abrasive grain movement trajectory

Fig. 4 illustrates the components of the PU-AP polishing system, which primarily include piezoelectric ceramics, a transformer, an inverter, a power supply, centrifugal stirring paddles, stirring paddles, and a micro-tapered hole workpiece.

3.2 Numerical model and boundary conditions

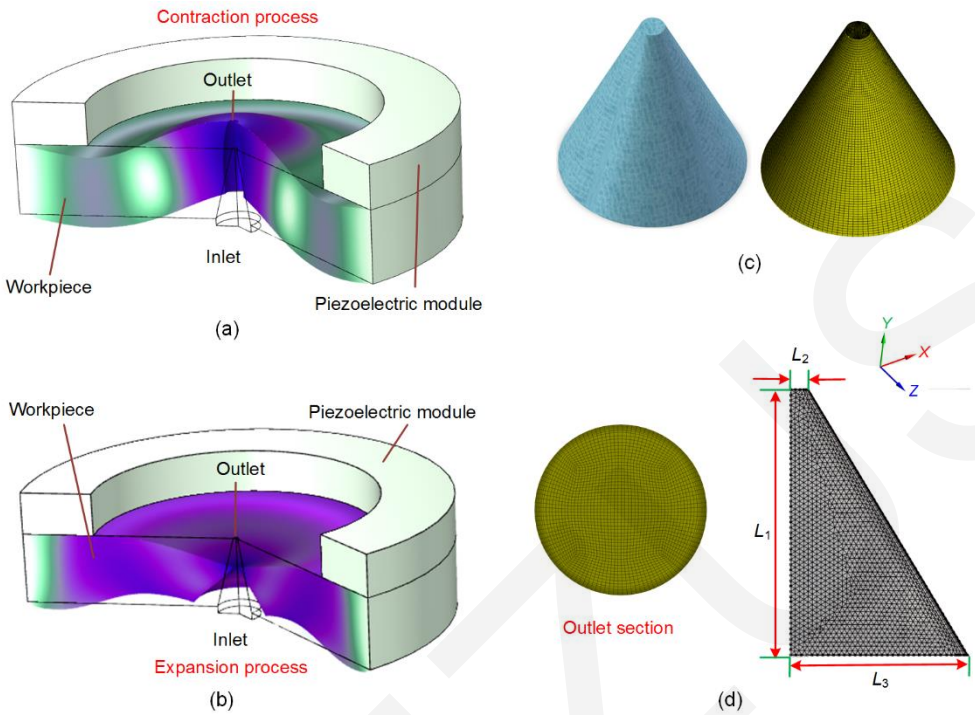

Fig. 5 Geometric model and constrained flow field for the PU-AP polishing method: (a) contraction process; (b) expansion process; (c) overall morphology of the micro-tapered hole and the meshing configuration; (d) outlet section and the grid cross-sectional view of micro-tapered hole. L_1: height; L_2: outlet radius; L_3: inlet radius

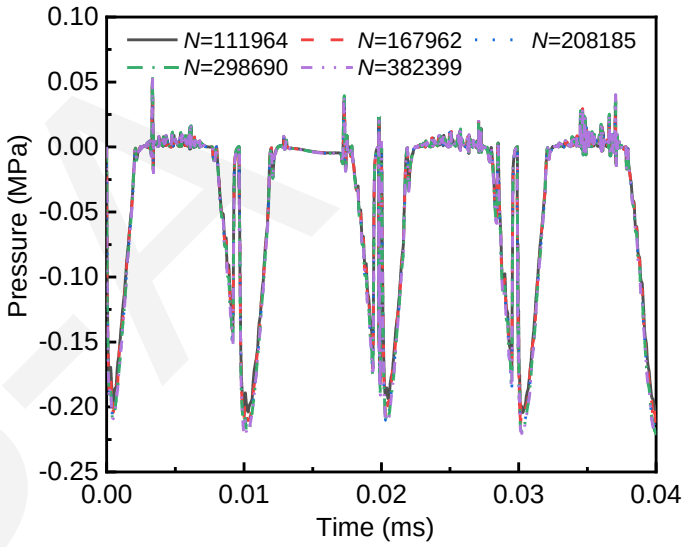

Fig. 6 Grid-unrelated validation (pressure–time distribution plots at multiple points)

Table 1 Physical parameters for the abrasive flow

Parameter	Value
Water density (kg/m³)	998
Water viscosity (Pa·s)	0.00103
SiO_2 density (kg/m³)	2200
SiO_2 diameter (μm)	0.06
SiO_2 volume fraction (%)	7
Inlet velocity (m/s)	10^{-6}
Hydraulic diameter (μm)	5.13
Main channel turbulence intensity (%)	5
Gravity acceleration (m/s²)	9.81

4 Numerical simulation results

4.1 Evolutionary mechanism of PU-AP expansion and contraction

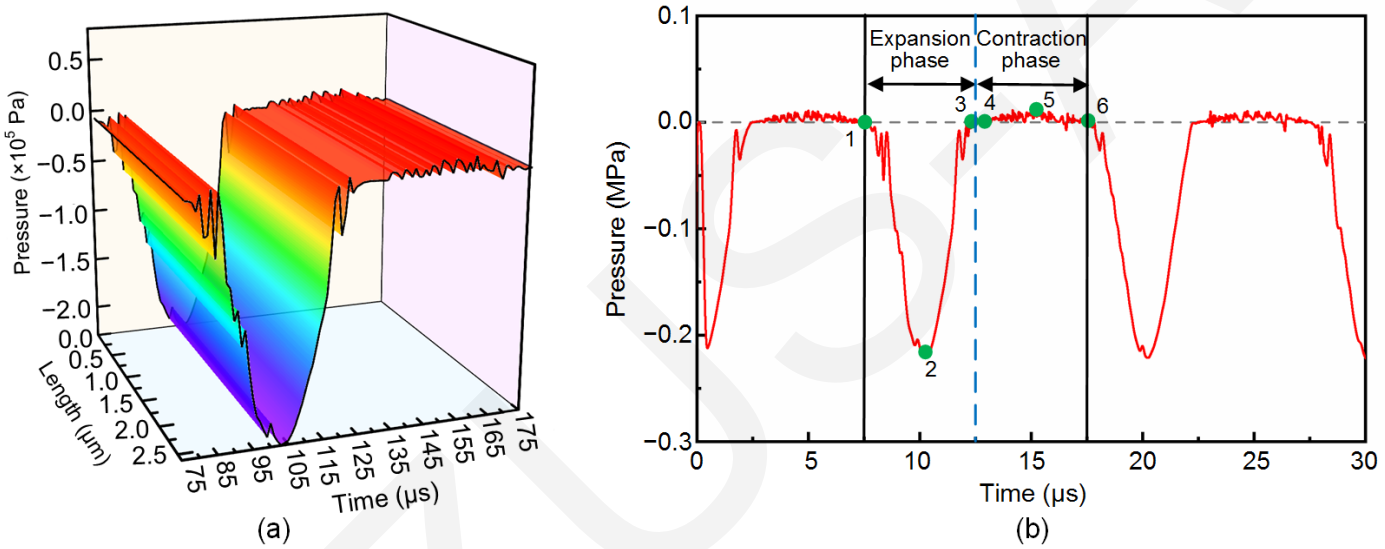

Fig. 7 Cyclical pressure variation curve on the wall surface of a micro-tapered hole: (a) first-cycle time–length–pressure 3D curve; (b) intermediate characteristic point pressure change rule

During the expansion and contraction of the PU-AP, the rapid fluctuations in the volume of the internal flow field result in elevated pressure and turbulent features. In order to predict the wall polishing effects, it is essential to examine the flow field characteristics of the inner wall surface. Fig. 6a displays the pressure distribution on the inner wall surface during the expansion and contraction cycle in a 3D graphic.

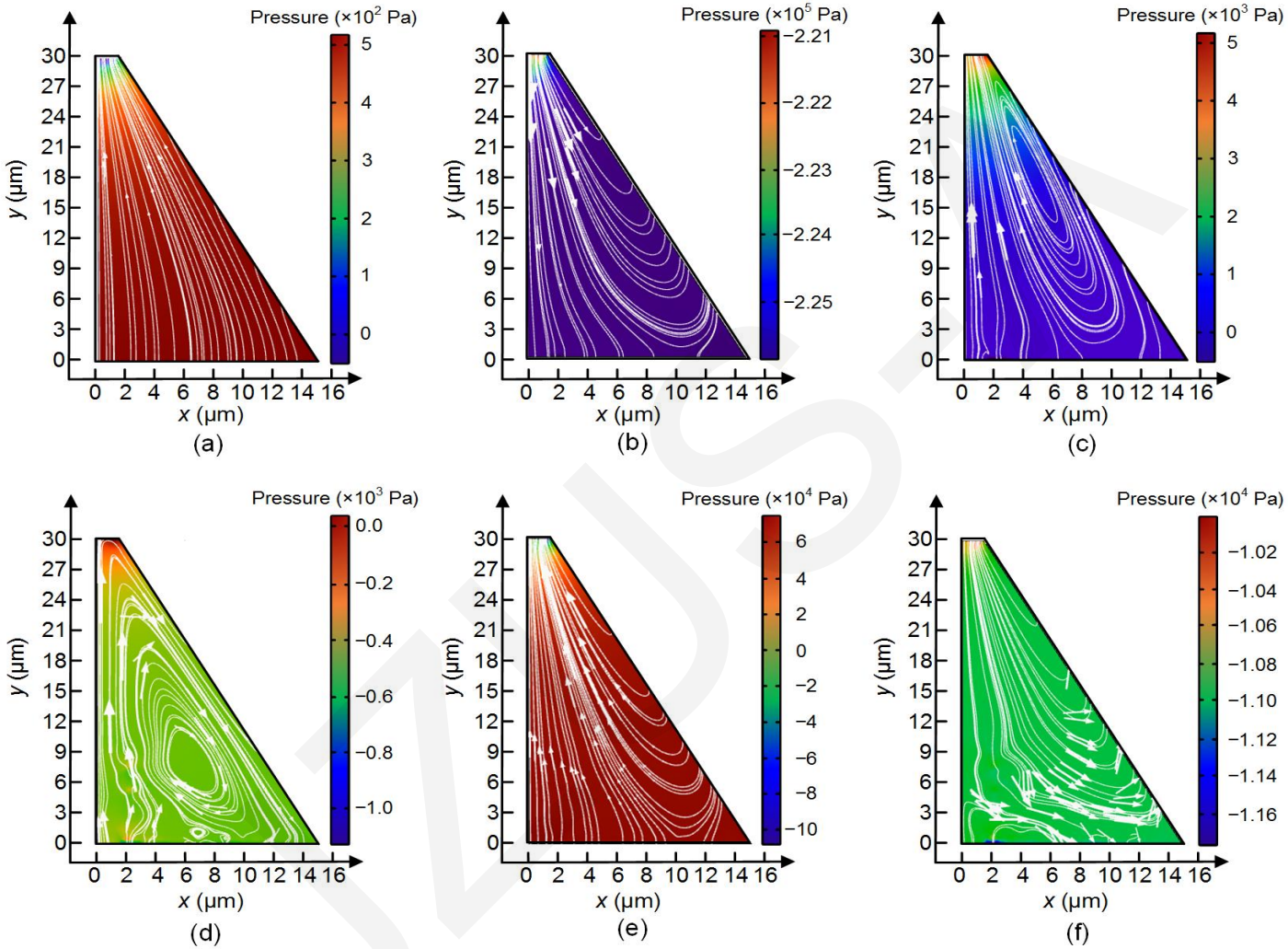

Fig. 8 Changes of flow field pressure and streamline patterns during the cycle: (a) Point 1; (b) Point 2; (c) Point 3; (d) Point 4; (e) Point 5; (f) Point 6. References to color refer to the online version of this figure

4.2 Collision process between PU-AP abrasive particles and the wall surface

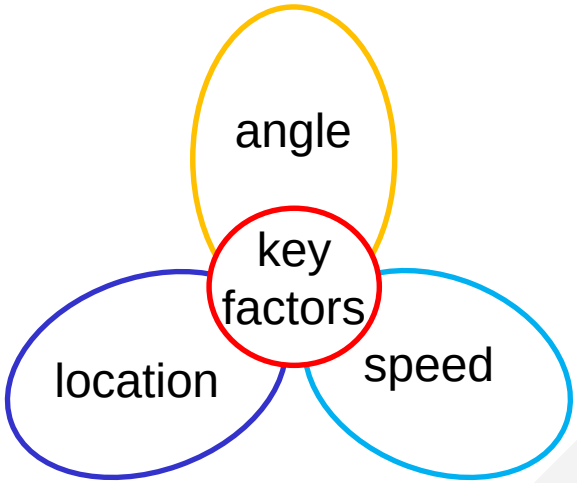

The key factors that affect the achieved level of polishing on the wall

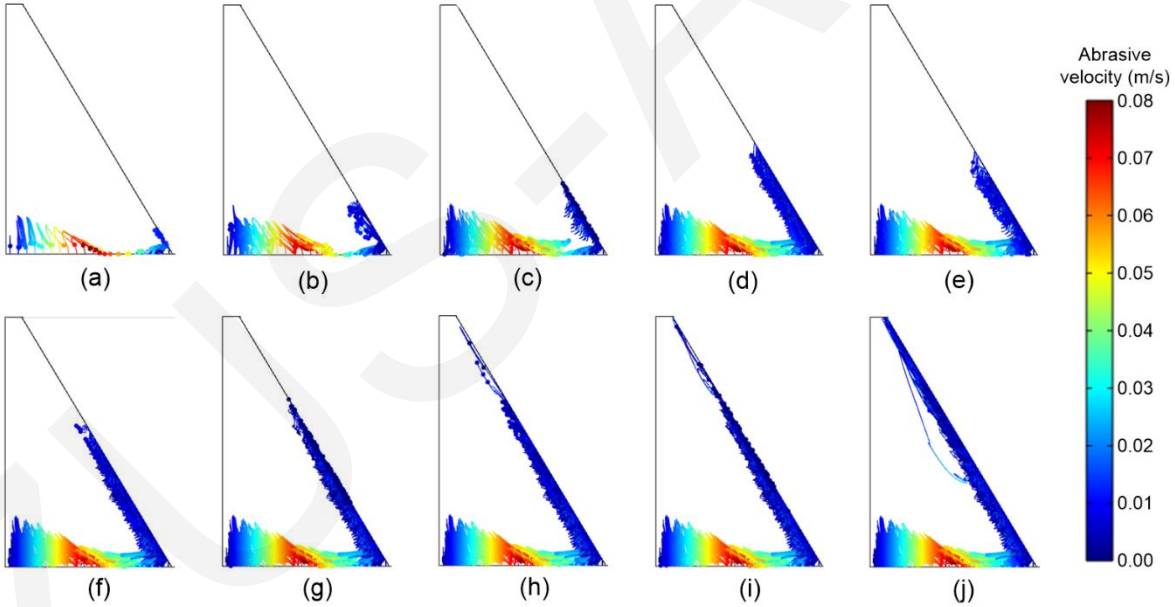

Fig. 9 Trajectory of the abrasive grains: (a) 0.0125 ms; (b) 0.025 ms; (c) 0.05 ms; (d) 0.075 ms; (e) 0.1 ms; (f) 0.125 ms; (g) 0.14 ms; (h) 0.145 ms; (i) 0.15 ms; (j) 0.2 ms. References to color refer to the online version of this figure

4.3 Effect of vibrational frequency and amplitude on the polished area

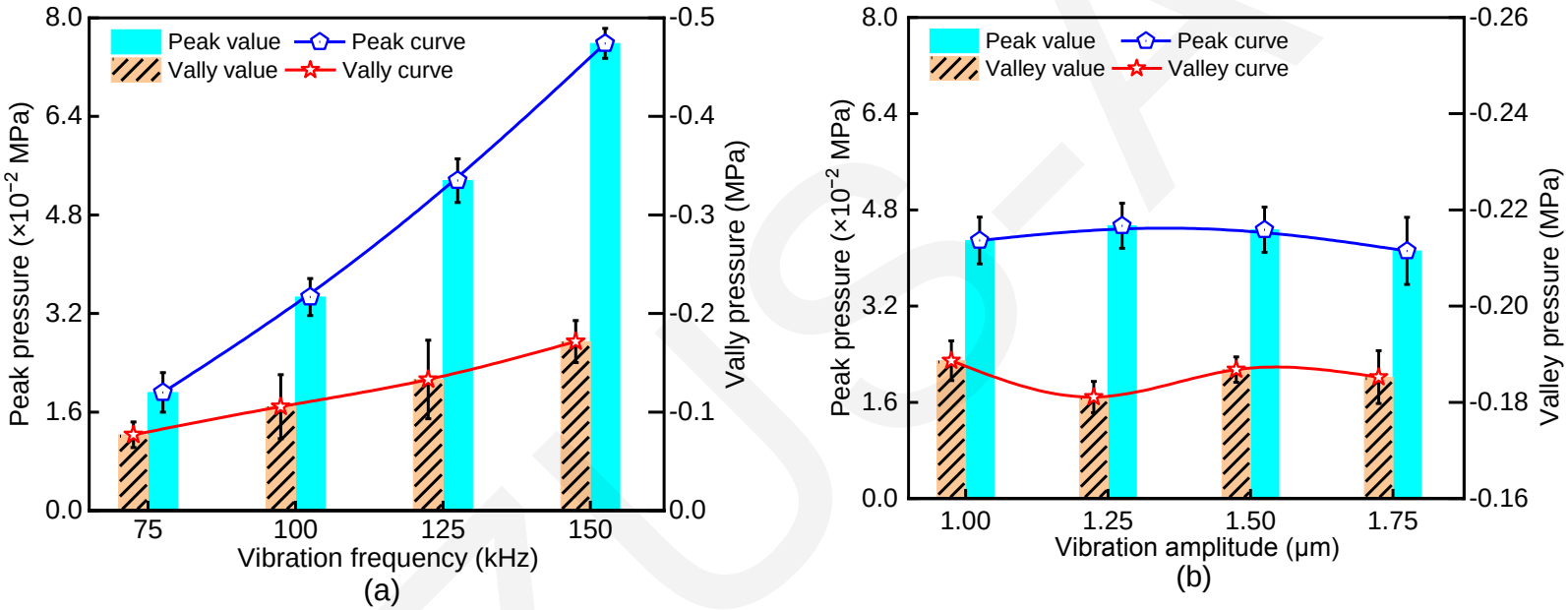

Fig. 10 Plot of vibration frequency, amplitude, and pressure variation: (a) variations of pressure peaks and valleys under different vibration frequencies; (b) variations of pressure peaks and valleys under different vibration amplitudes

4.3 Effect of vibrational frequency and amplitude on the polished area

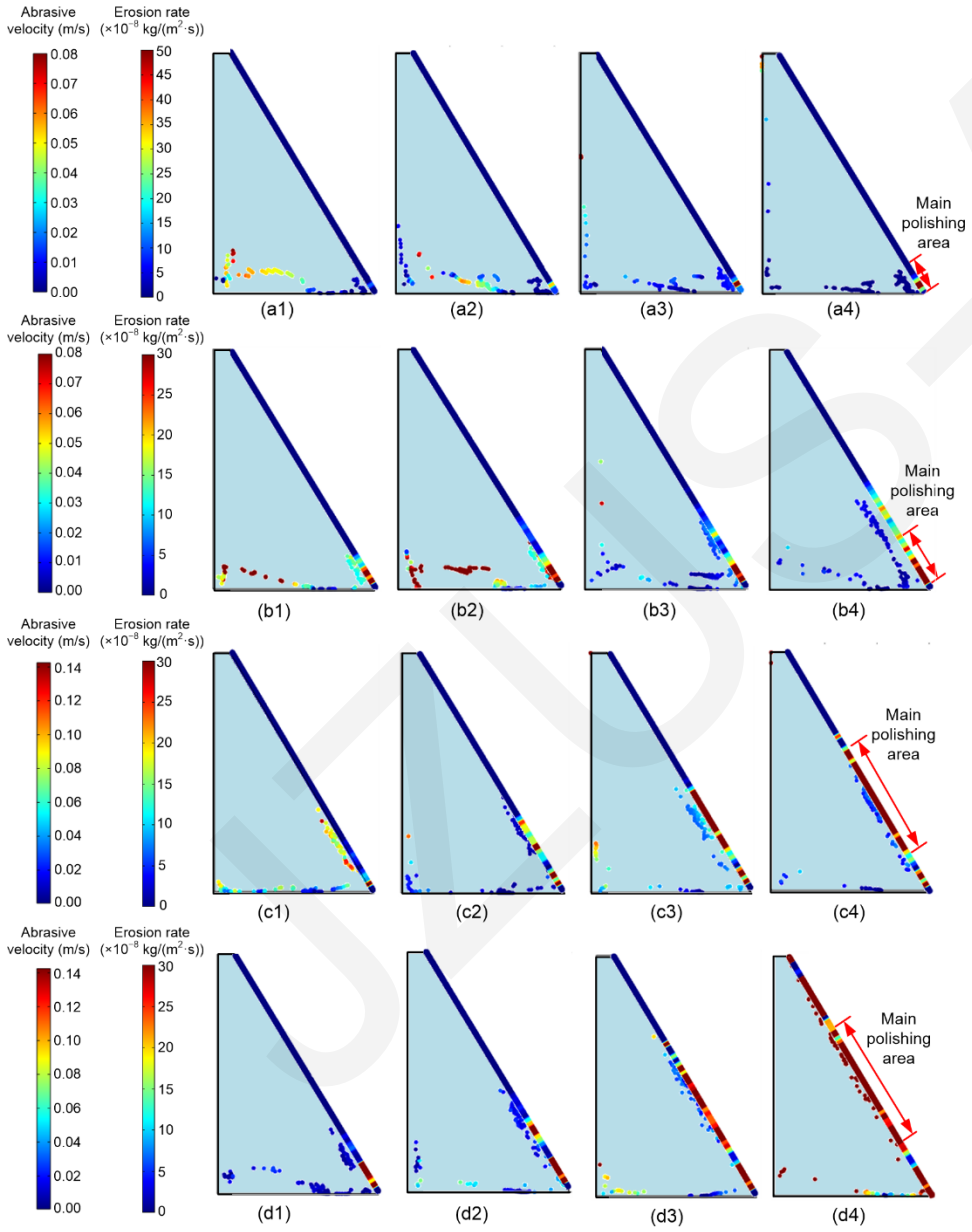

Fig. 11 Effect of vibrational frequency on flow field pressure, abrasive grain trajectory, and key polishing areas: (a1) 75 kHz, 0.025 ms; (a2) 75 kHz, 0.075 ms; (a3) 75 kHz, 0.125 ms; (a4) 75 kHz, 0.15 ms; (b1) 100 kHz, 0.025 ms; (b2) 100 kHz, 0.075 ms; (b3) 100 kHz, 0.125 ms; (b4) 100 kHz, 0.15 ms; (c1) 125 kHz, 0.025 ms; (c2) 125 kHz, 0.075 ms; (c3) 125 kHz, 0.125 ms; (c4) 125 kHz, 0.15 ms; (d1) 150 kHz, 0.025 ms; (d2) 150 kHz, 0.075 ms; (d3) 150 kHz, 0.125 ms; (d4) 150 kHz, 0.15 ms

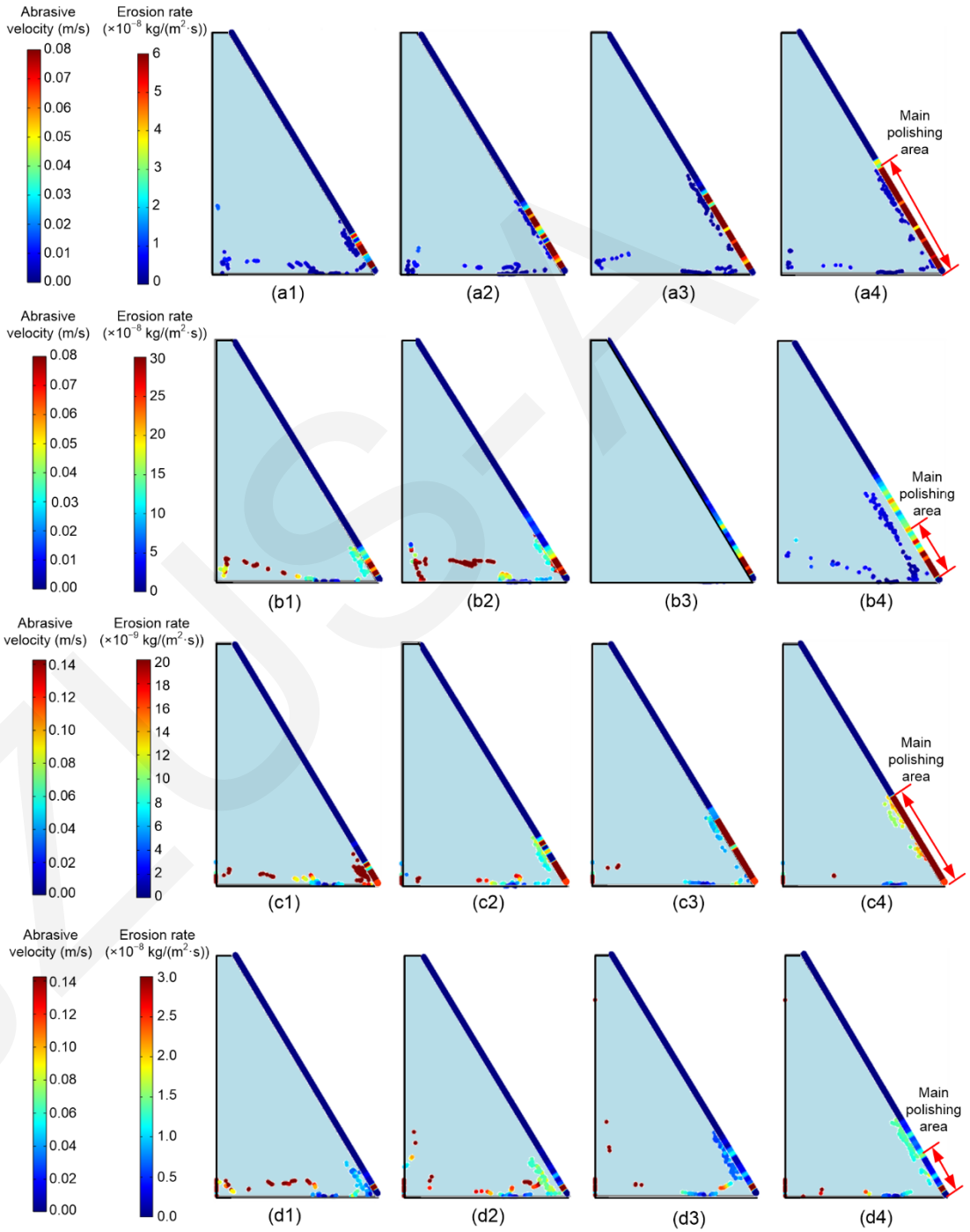

Fig. 12 Effect of vibrational amplitude on flow field pressure, abrasive grain trajectory, and key polishing areas: (a1) 1.95 μm, 0.025 ms; (a2) 1.95 μm, 0.075 ms; (a3) 1.95 μm, 0.125 ms; (a4) 1.95 μm, 0.15 ms; (b1) 2.44 μm, 0.025 ms; (b2) 2.44 μm, 0.075 ms; (b3) 2.44 μm, 0.125 ms; (b4) 2.44 μm, 0.15 ms; (c1) 3.05 μm, 0.025 ms; (c2) 3.05 μm, 0.075 ms; (c3) 3.05 μm, 0.125 ms; (c4) 3.05 μm, 0.15 ms; (d1) 3.81 μm, 0.025 ms; (d2) 3.81 μm, 0.075 ms; (d3) 3.81 μm, 0.125 ms; (d4) 3.81 μm, 0.15 ms

5 Construction of the PU-AP experimental platform

5.1 Experimental setup assembly

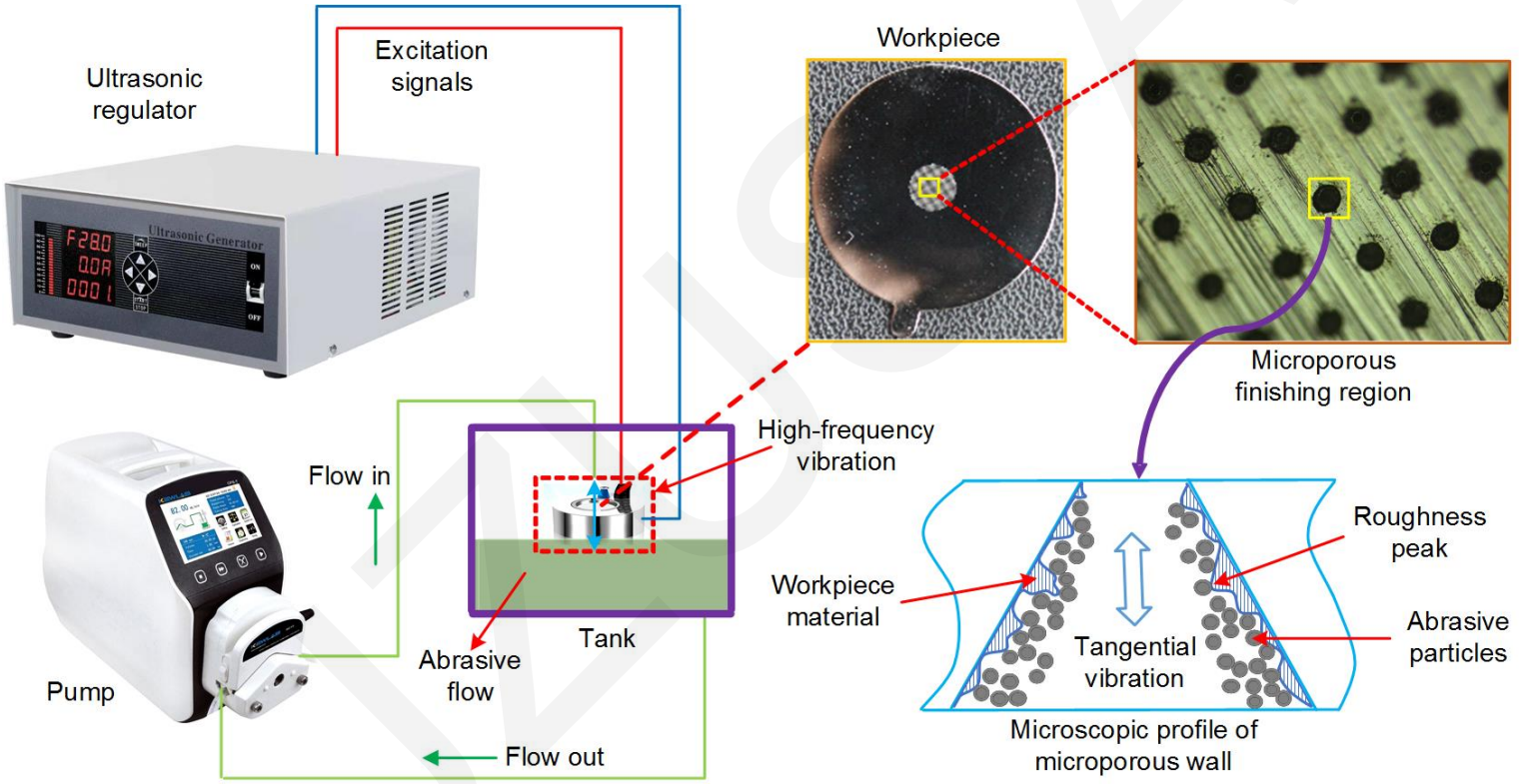

Fig. 13 Experimental workflow

5.2 Polishing experiment results

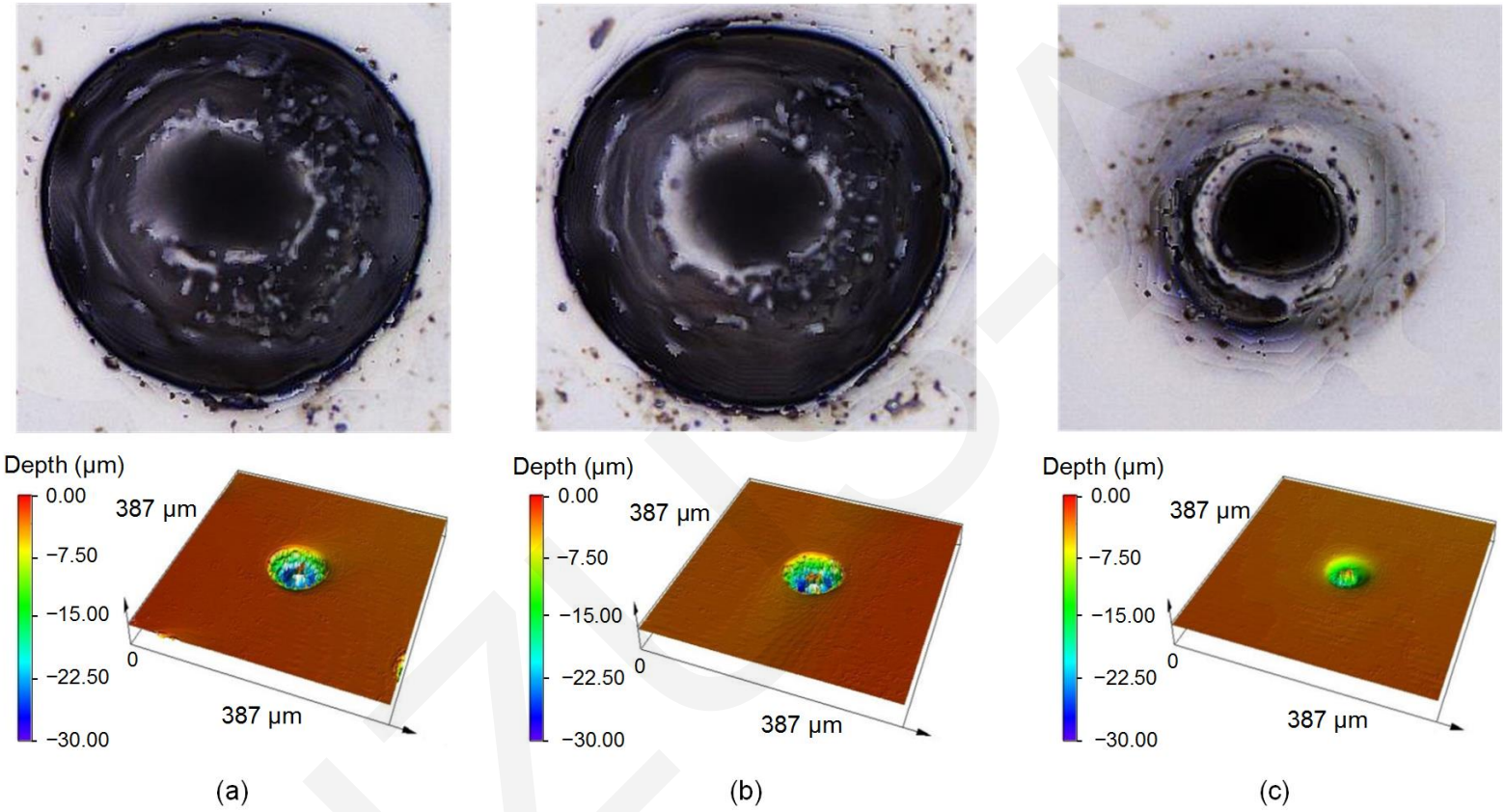

Fig. 14 Surface morphology of micro-tapered holes at different polishing moments: (a) unpolished; (b) after 4 h of polishing; (c) after 15 h of polishing

5.2 Polishing experiment results

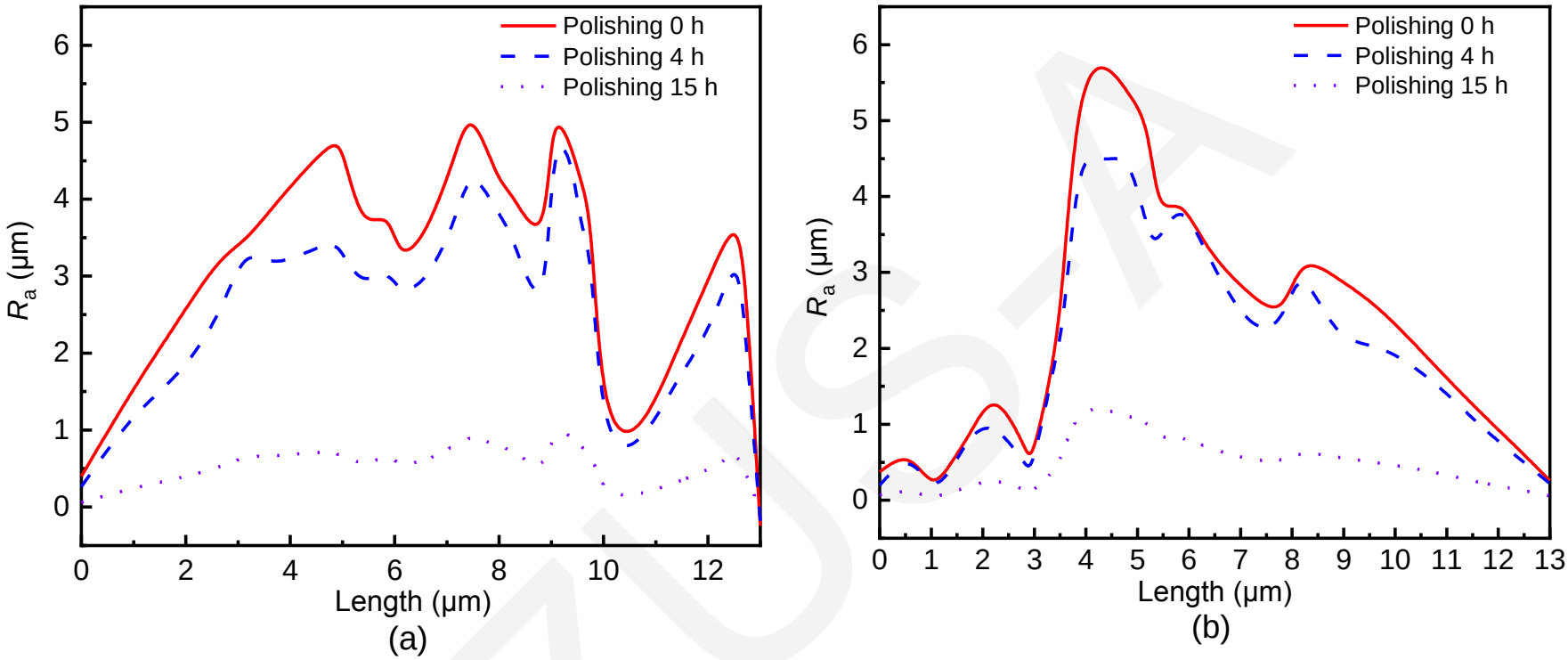

Fig. 15 Surface roughness (R_a) at different polishing moments: (a) left side; (b) right side

The primary objective of this study was to incorporate ultrasonic vibration into the polishing of wall surfaces in micro-tapered holes. Additionally, we aimed to uncover the phenomena of vortex formation, movement of abrasive grains, and erosion of the wall in conical hole cavities during the process of ultrasonic vibration coupling. Ultimately, utilizing the ultrasonic frequency and amplitude in the design allows for active control of the polishing area. However, PU-AP polishing techniques can still encounter difficulties in terms of material removal and vibrational fatigue effects; the material removal functionality could potentially be improved by pulsation and cavitation. These matters will be investigated in subsequent research.